Journal of Materials Chemistry A

PAPER

Influence of In doping on the thermoelectric properties of an $AgSbTe_2$ compound with enhanced figure of merit†

Cite this: *J. Mater. Chem. A*, 2014, **2**, 2839

Rajeshkumar Mohanraman,*[abc] Raman Sankar,[d] Karunakara Moorthy Boopathi,[ace] Fang-Cheng Chou,[de] Chih-Wei Chu,[e] Chih-Hao Lee[af] and Yang-Yuan Chen*[bg]

Received 6th November 2013
Accepted 10th December 2013

DOI: 10.1039/c3ta14547f

www.rsc.org/MaterialsA

A maximal thermoelectric figure-of-merit *ZT* for p-type $Ag(Sb_{1-x}In_x)Te_2$ samples with $x = 0.07$ is 1.35 at 650 K, yielding an enhancement of greater than 40% compared with that of an undoped $AgSbTe_2$ compound at the same temperature. This *ZT* enhancement can be primarily attributed to both the greatly enhanced power factor resulting from an increase in Seebeck coefficient because of the increase in the effective mass and the substantial decrease in thermal conductivity which could be ascribed to the enhancement of the phonon scattering mechanism by dopants with different atomic weights. These results indicate that doping with In is effective for enhancing the thermoelectric performance of the p-type $AgSbTe_2$ compound.

1. Introduction

The worldwide concern over reliance on fossil fuels drives the need for alternative energy sources and novel energy conversion techniques, among which the thermoelectric (TE) technique possesses several unique features such as an entirely solid-state assembly, ease of switching between power generation mode (based on the Seebeck effect) and refrigeration mode (based on the Peltier effect), low cost maintenance and compatibility with other energy conversion devices. TE effects enable the direct conversion between thermal and electrical energy and provide an alternate route for waste heat recovery and environmentally friendly refrigeration.[1–3] The performance of TE devices is assessed using the dimensionless figure of merit $ZT = \alpha^2\sigma T/\kappa$, where α, σ, T, and κ are the Seebeck coefficient, the electrical conductivity, the absolute temperature, and the thermal conductivity, respectively. Because α, σ, and the electronic contribution to κ involve band structures (*e.g.*, energy gap E_g, effective mass carrier m^*) and scattering mechanisms, controlling the parameters independently is difficult.[1] Therefore, a *ZT* value of 1 has long been considered a benchmark for assessing numerous TE materials. Based on the above relationship, optimally performing TE materials should possess high electrical conductivity, a large Seebeck coefficient, and low thermal conductivity.[1]

Ternary chalcogenide $AgSbTe_2$ has been widely reported as a promising TE material[4–10] because it exhibits relatively low thermal conductivity (0.6–0.7 $W\,m^{-1}\,K^{-1}$).[11–14] $AgSbTe_2$ is known for comprising a disordered NaCl-type structure ($Fm\bar{3}m$) in which Ag and Sb randomly occupy the Na site.[15] Because of the complex ordering of Ag/Sb on the face-centered cubic lattice, the electronic properties of $AgSbTe_2$ exhibit anomalies. Diffuse reflectance measurements yield a band gap of approximately 0.35 eV, whereas the electrical conductivity suggests a strongly degenerate behavior. Studies on atomic ordering and gap formation in Ag–Sb based ternary chalcogenides have indicated that the anomalous electronic properties of $AgSbTe_2$ can be caused by a small intrinsic band gap and shallow impurity states.[12] Recent advancements in combining cubic $AgSbTe_2$ with other compounds have enabled the development of nanostructured TE materials, such as $(AgSbTe_2)_{1-x}(PbTe)_x$ (LAST)[16–19] and $(AgSbTe_2)_{1-x}(GeTe)_x$ (TAGS),[20,21] with excellent TE properties.

Doping is a potential approach to optimize the thermoelectric properties of p-type $AgSbTe_2$ by reducing its thermal conductivity and adjusting its carrier concentration. In this study, trivalent In^{3+} ions were selected to substitute Sb^{3+} ions in a p-type $Ag(Sb_{1-x}In_x)Te_2$ system to dramatically suppress lattice thermal conductivity and simultaneously contribute to the total charge-carrier concentration. In the present study, the role of In

[a]*Department of Engineering and System Science, National Tsing Hua University, Taiwan, Republic of China. E-mail: rajeshx@phys.sinica.edu.tw; Fax: +886-2-2783-4187; Tel: +886-2-2789-6725*

[b]*Institute of Physics, Academia Sinica, Taiwan, Republic of China. E-mail: cheny2@phys.sinica.edu.tw*

[c]*Nano Science and Technology, Taiwan International Graduate Program, Academia Sinica, Taiwan, Republic of China*

[d]*Center for Condensed Matter Sciences, National Taiwan University, Taiwan, Republic of China*

[e]*Research Center for Applied Science, Academia Sinica, Taiwan, Republic of China*

[f]*National Synchrotron Radiation Research Center, Taiwan, Republic of China*

[g]*Graduate Institute of Applied Physics, National Chengchi University, Taiwan, Republic of China*

† Electronic supplementary information (ESI) available. See DOI: 10.1039/c3ta14547f

substitution on the TE properties of $Ag(Sb_{1-x}In_x)Te_2$ ($x = 0$, 0.03, 0.05, and 0.07) at 300 to 700 K was investigated. Thus, the influence of In-doping on the thermodynamic properties, microstructure, and TE transport behavior of $Ag(Sb_{1-x}In_x)Te_2$ (*i.e.* $x > 0$, hereinafter referred to as In-AST) samples was systematically investigated in this study.

2. Experimental

High purity raw materials, Ag (99.999%, shot), Sb (99.9999%, shot), In (99.999%, shot) and Te (99.999%, shot), were weighed according to the stoichiometric ratio of $Ag(Sb_{1-x}In_x)Te_2$ ($x = 0$, 0.03, 0.05, and 0.07) and then sealed into carbon-coated quartz tubes with a diameter of 13 mm under high vacuum (10^{-3} torr). The quartz tube was heated at 1073 K for 10 h (including rocking to facilitate complete mixing and homogeneity of the liquid phase) and then cooled to 773 K over 6 days and finally followed by cooling to room temperature over 10 h. Highly dense ingots with a dark silvery metallic shine were obtained. These ingots which were stable in water and air were then cut and polished into approximately $3 \times 3 \times 12$ mm^3 rectangular shapes, and circular discs with 12 mm diameters and thicknesses 1–2 mm for later physical property measurements. The density of the ingots measured using the Archimedes method varied from 7.11 to 7.12 g cm^{-3}, which is greater than 99.9% of the theoretical density.

X-ray diffraction spectra analysis was conducted for phase identifications by using a powder X-ray diffractometer (XRD; X'Pert PRO-PANalytical, CuKα radiation) at 2θ angles of 20–80°. With these data, the lattice parameters of $Ag(Sb_{1-x}In_x)Te_2$ ($x = 0$, 0.03, 0.05, and 0.07) samples were calculated using the Rietveld refinement program. The microstructure of the sample with $x = 0.07$ was investigated using field emission scanning electron microscopy (FESEM; Hitachi, S-4800). The chemical composition of the as-prepared ingots was determined using wavelength dispersive X-ray fluorescence spectrometry (WD-XRF; Rigaku, ZSX primus II). To investigate the optical energy gap of these series, the optical diffuse reflectance measurements[22–24] were performed on finely ground powders using a Fourier transform infra-red spectrometer (FTIR, Nicolet 6700) at room temperature. The room temperature Hall effect measurements were conducted using a four-probe configuration (ECOPIA, HMS-5000). The electrical conductivity σ and Seebeck coefficient α were measured simultaneously using commercial equipment (ZEM-3, ULVAC-RIKO, Japan) in a He atmosphere from 300 to 700 K. The thermal conductivity κ was calculated using the equation $\kappa = D \times C_p \times d$ based on the thermal diffusivity D obtained using a laser flash apparatus (NETZSCH, LFA 457); the specific heat C_p was determined using a differential scanning calorimeter (DSC, NETZSCH, STA 449), and the density d was obtained using the Archimedes method. The overall measurement errors in the σ, α, and κ are ±2%, ±3% and ±3% respectively, producing a maximum of approximately 11% in the ZT calculation.

3. Results and discussions

Crystalline ingots of $Ag(Sb_{1-x}In_x)Te_2$ were cut and polished for measuring the transport properties. Fig. 1a presents the powder XRD patterns of the samples with the composition $Ag(Sb_{1-x}In_x)$

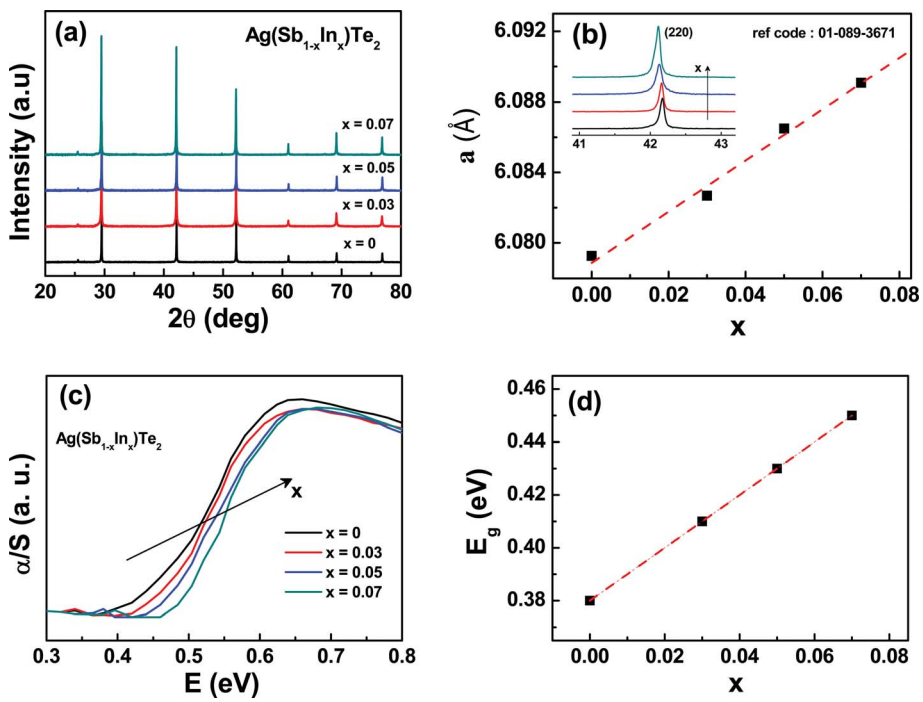

Fig. 1 (a) Powder XRD patterns of $Ag(Sb_{1-x}In_x)Te_2$ samples ($x = 0$, 0.03, 0.05, and 0.07), (b) composition dependence of lattice parameters fitted using the Rietveld method (the inset shows the enlarged XRD peak shifting) for $Ag(Sb_{1-x}In_x)Te_2$, (c) Infrared absorption spectra, and (d) composition dependence of the energy gap of the $Ag(Sb_{1-x}In_x)Te_2$ samples.

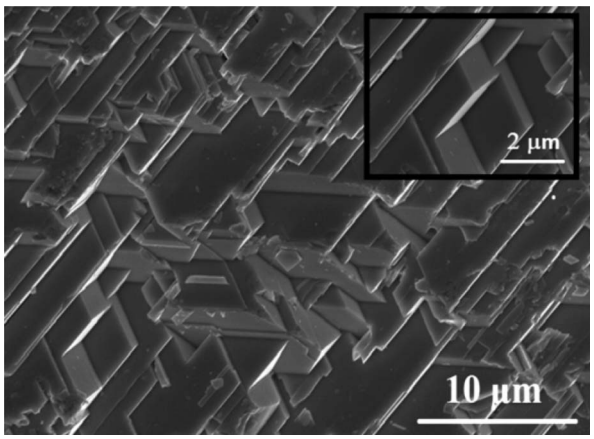

Fig. 2 FESEM image of the bulk $Ag(Sb_{0.93}In_{0.07})Te_2$. The inset shows a magnified portion.

Te_2 ($x = 0$, 0.03, 0.05, and 0.07). All of the diffraction peaks were indexed to the face-centered cubic $AgSbTe_2$ structure (reference code: 01-089-3671) without any indication of secondary phase impurities. The lattice parameter "a" was calculated using Reitveld refinement; as shown in Fig. 1b, the lattice parameter increased when the In content increased, which was expected based on the difference between the ionic radii of In^{3+} (0. 81 Å) and Sb^{3+} (0. 76 Å), also follows Vegard's law (shown as a red dashed line). The enlarged (220) peaks clearly show a gradual shift to lower angles as the In content increased; as shown in the inset of Fig. 1b, both indicate that In substitutes Sb in the $AgSbTe_2$ crystal lattice. The spectroscopically measured optical energy band gap of the bulk $AgSbTe_2$ is ~0.38 eV which is a typical narrow band gap semiconductor (Fig. 1c); this is consistent with the previous electronic band structure calculation for $AgSbTe_2$.[25] The systematic increase in the band gaps of the In-AST samples compared to undoped $AgSbTe_2$ is shown in Fig 1d, which verifies that In successfully substituted Sb in a sublattice of $AgSbTe_2$. The results from both the lattice parameter and band gap follow Vegard's law (shown as red dashed lines in Fig. 1b and d) and support good solubility of In doping in the $AgSbTe_2$ system.

The microstructure of all of the samples shows the same morphology. Fig. 2 shows the FESEM image of the fracture-free surface of the $Ag(Sb_{0.93}In_{0.07})Te_2$ sample. The magnified image (inset of Fig. 2) shows a highly compact structure, which is in agreement with the density measurements. The composition variation of the $Ag(Sb_{1-x}In_x)Te_2$ series obtained using wavelength dispersive X-ray fluorescence analysis was in good agreement with those of the nominal compositions (see the ESI, Table S1 and also Fig. S1–S4†).

The temperature dependence of the electrical conductivity σ was measured within the range of 300 to 700 K (Fig. 3a). As expected, the sample with a low electrical conductivity exhibited a high Seebeck coefficient α, and the trend of α *versus* T curve is reflected from that of the σ *versus* T curve in Fig. 3a and c, respectively. For all of the samples, the electrical conductivity decreased with increasing temperature for $T < 600$ K and then slightly increased at $T > 600$ K, indicating the behavior of a typical degenerate or heavily doped semiconductor. Fig. 3b shows the carrier concentrations (n_H) and Hall mobilities (μ_H) of the $Ag(Sb_{1-x}In_x)Te_2$ samples at room temperature as a function of In content. The n_H for In-AST samples shows a declining trend with the In content x because of a slight

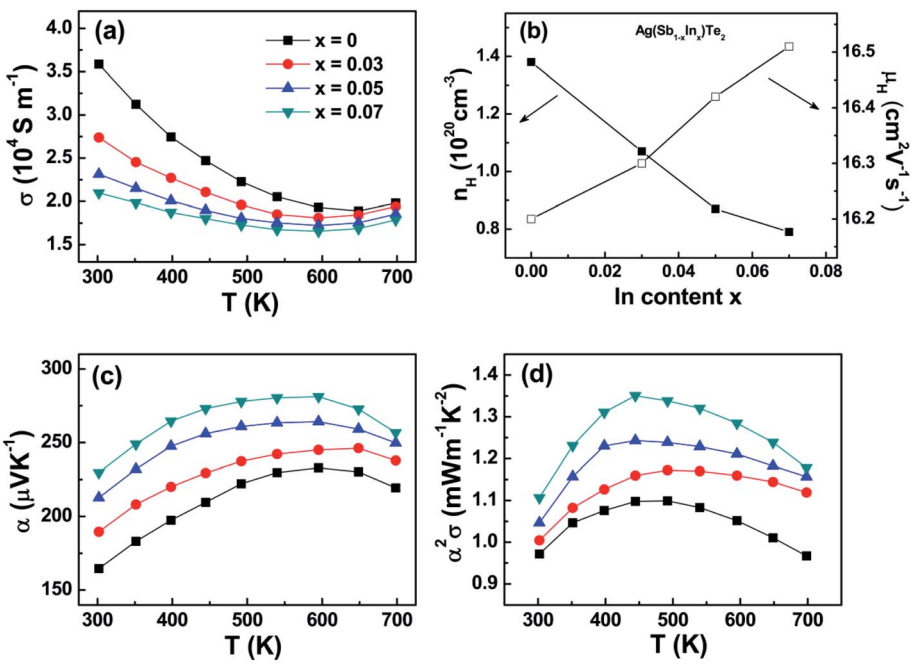

Fig. 3 Temperature dependence of the electrical transport properties of the $Ag(Sb_{1-x}In_x)Te_2$ samples (a) electrical conductivity, (b) room temperature carrier concentration n_H and mobility μ_H as a function of In content 'x', (c) Seebeck coefficient, and (d) power factor.

Table 1 Carrier concentration n, Hall mobility μ_H, electrical conductivity σ, Seebeck coefficient α, effective mass m^*/m_0 and Lorentz values L of $Ag(Sb_{1-x}In_x)Te_2$ samples at 300 K

Nominal composition	XRF composition	n (10^{20} cm^{-3})	μ_H (cm^2 V^{-1} s^{-1})	σ (10^4 S m^{-1})	α (μV K^{-1})	m^*/m_0	L
$AgSbTe_2$	$AgSb_{0.9}Te_{2.01}$	1.38	16.2	3.6	165	2.08	1.71
$Ag(Sb_{0.97}In_{0.03})Te_2$	$Ag(Sb_{0.96}In_{0.037})Te_{2.01}$	1.07	16.3	2.7	190	2.09	1.72
$Ag(Sb_{0.95}In_{0.05})Te_2$	$Ag(Sb_{0.93}In_{0.06})Te_{2.02}$	0.87	16.42	2.3	212	2.10	1.73
$Ag(Sb_{0.93}In_{0.07})Te_2$	$Ag(Sb_{0.91}In_{0.08})Te_{2.02}$	0.79	16.51	2.1	230	2.12	1.74

increase in the energy band gap (shown in Fig. 1d). The μ_H increases with In content, which could be due to the decreased scattering by lower electron concentration. However, the decrease in the carrier concentration is larger than the carrier mobility increase; this is why the electrical conductivity decreases with In content. Table 1 shows the properties used to describe the electron transport characteristics of In-doped $Ag(Sb_{1-x}In_x)Te_2$ compounds at room temperature. Compared with the undoped $AgSbTe_2$, the In-AST samples displayed a lower carrier concentration but higher mobility.

The Seebeck coefficients of all the specimens were positive (Fig. 3c), indicating the p-type conduction. At room temperature, the Seebeck coefficients for the In-AST samples ranged from 190–230 μV K^{-1}, which is higher than that of the undoped $AgSbTe_2$ sample. The increased Seebeck coefficient and the decreased electrical conductivity of the In-AST samples can be ascribed to the decreased carrier concentration caused by In-doping. The Seebeck coefficient of metals or degenerate semiconductors, with the assumption of a parabolic band and energy independent scattering, can be expressed as[26,27]

$$\alpha = \frac{8\pi^2 k_B^2 T}{3qh^2} m^* \left(\frac{\pi}{3n}\right)^{2/3} \quad (1)$$

where n is the carrier concentration, k_B is the Boltzmann constant, q is the electronic charge, h is the Planck constant, and m^* is the effective mass. The effective masses were calculated with eqn (1) and listed in Table 1. In this work, the maximum Seebeck coefficient value of 230 μV K^{-1} was obtained for the sample ($x = 0.07$) with a maximum effective mass value of $2.12m_0$ at room temperature. So, we can suggest that the increase of the effective mass is the reason for the increase of the Seebeck coefficient. The power factor PF $= \alpha^2\sigma$ and the curves are plotted in Fig. 3d. The samples with $x = 0.07$ exhibited the highest PF among all of the samples with a peak PF value of 1.35×10^{-3} W m^{-1} K^{-2} at 450 K.

The thermal diffusivity D and specific heat capacity measurements of the $AgSb(Sn_xTe_{2-x})$ samples at constant pressure C_p are shown in Fig. 4a. Based on the specific heat data, the results closely match the C_p value of $AgSbTe_2$ reported in the literature[13] (approximately ~0.205 J g^{-1} K^{-1}). The total thermal conductivity was calculated as a product of C_p, D, and d. Fig. 4b shows the temperature dependence of the total thermal conductivity κ of the $Ag(Sb_{1-x}In_x)Te_2$ samples. For all of the samples, the κ first decreased and subsequently increased when the temperature increased, and the magnitude spanned from 0.58 to 0.81 W m^{-1} K^{-1}. In-AST samples exhibited lower thermal

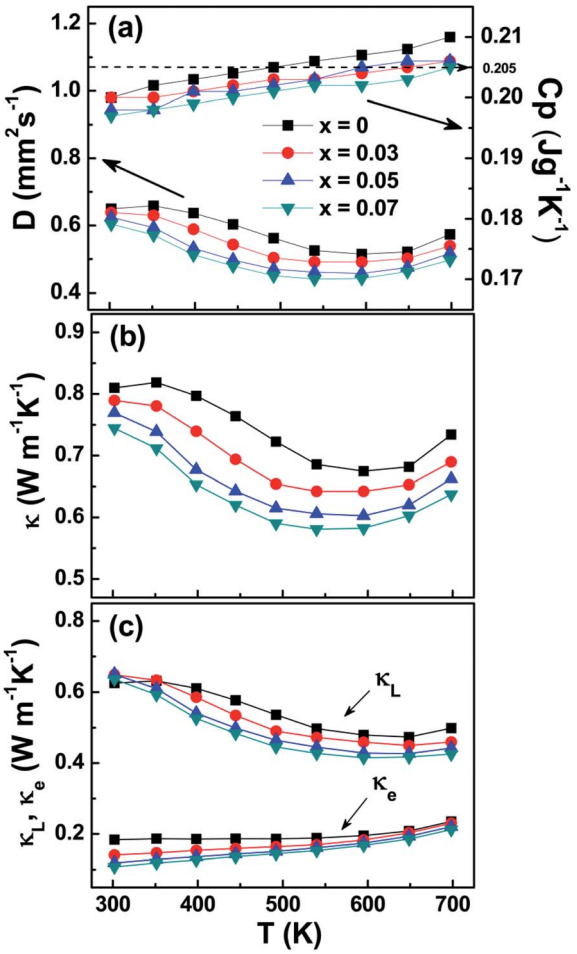

Fig. 4 Temperature dependence of (a) diffusivity and specific heat capacity, (b) total thermal conductivity and (c) lattice and electronic thermal conductivity of $Ag(Sb_{1-x}In_x)Te_2$ samples ($x = 0$, 0.03, 0.05, and 0.07).

conductivities than the undoped $AgSbTe_2$ sample did. Using the Wiedmann–Franz law, $\kappa_e = L\sigma T$, where L is the Lorentz number, the lattice thermal conductivity κ_L can be estimated by subtracting the electronic thermal conductivity κ_e from the total thermal conductivity κ, $\kappa_L = \kappa - L\sigma T$. The room temperature L values are listed in Table 1 and the calculation details are shown in the ESI.† κ_e was estimated to be less than 20% of κ for In-AST samples for all of the temperatures used (Fig. 4c), indicating that the κ of the In-AST samples was mainly determined by phonon transport. Moreover, κ_L decreased as In content increased, which

may be caused by both the enhanced phonon scattering of the dopant and the decreased carrier concentrations (Fig. 4c). The sample with $x = 0.07$ exhibited the lowest lattice thermal conductivity (0.41 W m^{-1} K^{-1}) compared with that of the undoped $AgSbTe_2$ (0.48 W m^{-1} K^{-1}) at 600 K, close to the minimal theoretical thermal conductivity (0.3 W m^{-1} K^{-1}) calculated using formulae reported by Cahill *et al.*[28] The possible reason for the substantial decrease in lattice thermal conductivity achieved in the In-AST samples can be attributed to the lattice mismatch generated by substituting In for Sb in the $AgSbTe_2$ system, which prompted the mass fluctuation scattering and strain field fluctuation scattering of phonons caused by the mass and size differences between the alloying atoms and host atoms.[29–32] This increases the anharmonicity of the lattice vibrational spectrum which enhances effective phonon scatterings by affecting the disordered Ag/Sb lattice in the $AgSbTe_2$ system and a decline in lattice thermal conductivities is expected.

The dimensionless TE figure of merit ZT was calculated based on the measured values of σ, α, and κ using the equation $ZT = \alpha^2\sigma T/\kappa$. Fig. 5 shows the temperature dependence of the ZTs of all the $Ag(Sb_{1-x}In_x)Te_2$ samples ($x = 0$, 0.03, 0.05 and 0.07). Whereas the values of ZT of all samples were comparable at room temperatures, the benefit of In-doping is more clearly demonstrated at elevated temperatures. The highest ZT among all of the samples was observed in $Ag(Sb_{0.93}In_{0.07})Te_2$, which reached $ZT = 1.35$ at 650 K because of its relatively enhanced PF and lowest thermal conductivity at high temperatures. As we know, the average ZT (ZT_{avg}) enables the efficiency of the thermoelectric generator to be accurately evaluated. The ZT_{avg} value calculated in the temperature range of 300 to 700 K as shown in the inset of Fig. 5 is about 1.02, also much higher than those of the Pb ($ZT_{avg} = 0.58$)[33] and Sn ($ZT_{avg} = 0.63$)[34] doped samples and comparable to the Se ($ZT_{avg} = 1.03$)[12] and Na ($ZT_{avg} = 1.1$)[11] doped samples in the same temperature range. This result indicates that In-doped $AgSbTe_2$ samples are more desirable for energy recovery from waste heat in a medium temperature range.

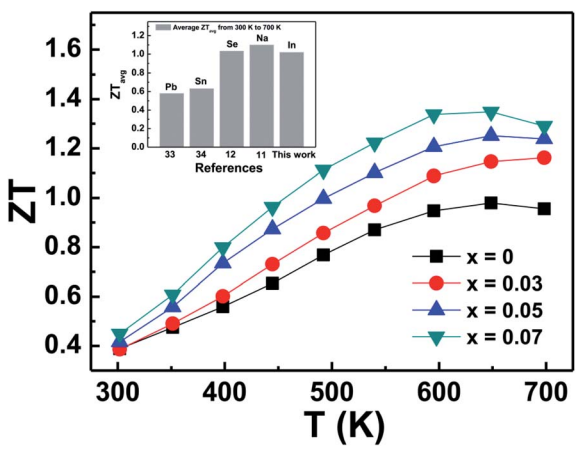

Fig. 5 Temperature dependence of the thermoelectric figure of merit ZT of the $Ag(Sb_{1-x}In_x)Te_2$ samples ($x = 0$, 0.03, 0.05, and 0.07). The inset shows the average ZT_{avg} calculated in the temperature range from 300 to 700 K. Data of the samples doped with Pb, Sn, Se and Na are found in the literature.[11,12,33,34]

4. Conclusions

In summary, the TE properties of In-doped $Ag(Sb_{1-x}In_x)Te_2$ compounds were investigated. XRD analysis indicated that single-phase materials crystallize in a cubic NaCl-type structure in In-doped $AgSbTe_2$ samples. The lattice thermal conductivities were reduced substantially which could be ascribed to the enhancement of phonon scattering caused by the dopants having dissimilar atomic weights with those of the host atoms, and the PFs were greatly enhanced because of the increase in Seebeck coefficient (compared with that of the undoped $AgSbTe_2$). The optimal TE performance was achieved using the sample with $x = 0.07$, because substituting In for Sb led to an increased carrier concentration and enhanced phonon scattering. A maximal ZT value of 1.35 was achieved at 650 K for the $Ag(Sb_{0.97}In_{0.03})Te_2$ sample, which is 40% higher than that of the undoped $AgSbTe_2$ at the same temperature. To ensure the thermal stability of the In-AST samples at elevated temperatures, the samples were annealed at 723 K for 5 days. After annealing, the ZT values at 700 K demonstrated almost no changes (Fig. S5, ESI†). These results suggest that the $Ag(Sb_{1-x}In_x)Te_2$ system with $x = 0.07$ has potential applications in TE power generation in the medium temperature range.

Acknowledgements

This work was supported by Academia Sinica and the National Science Council, Taiwan, Republic of China, Grant no. NSC100-2112-M-001-019-MY3.

References

1 M. Zebarjadi, K. Esfarjani, M. S. Dresselhaus, Z. F. Ren and G. Chen, *Energy Environ. Sci.*, 2012, **5**, 5147–5162.
2 J. P. Heremans, B. Wiendlocha and A. M. Chamoire, *Energy Environ. Sci.*, 2012, **5**, 5510–5530.
3 W. Zhou, W. Zhao, Z. Lu, J. Zhu, S. Fan, J. Ma, H. H. Hng and Q. Yan, *Nanoscale*, 2012, **4**, 3926–3931.
4 S. N. Zhang, T. J. Zhu, S. H. Yang, C. Yu and X. B. Zhao, *Acta Mater.*, 2010, **58**, 4160–4169.
5 H. Wang, J. F. Li, M. Zhou and T. Sui, *Appl. Phys. Lett.*, 2008, **93**, 202106.
6 J. Xu, H. Li, B. Du, X. Tang, Q. Zhang and C. Uher, *J. Mater. Chem.*, 2010, **20**, 6138–6143.
7 S. N. Zhang, T. J. Zhu, S. H. Yang, C. Yu and X. B. Zhao, *J. Alloys Compd.*, 2010, **499**, 215–220.
8 J. D. Sugar and D. L. Medlin, *J. Alloys Compd.*, 2009, **478**, 75–82.
9 H. A. Ma, T. C. Su, P. W. Zhu, J. G. Guo and X. P. Jia, *J. Alloys Compd.*, 2008, **454**, 415–418.
10 D. L. Medlin and J. D. Sugar, *Scr. Mater.*, 2010, **62**, 379–382.
11 B. L. Du, H. Li and X. F. Tang, *J. Alloys Compd.*, 2011, **509**, 2039–2043.
12 B. Du, H. Li, J. Xu, X. Tang and C. Uher, *Chem. Mater.*, 2010, **22**, 5521–5527.
13 D. T. Morelli, V. Jovovic and J. P. Heremans, *Phys. Rev. Lett.*, 2008, **101**, 035901.

14 E. F. Hockings, *Phys. Chem. Solids*, 1959, **10**, 341.
15 R. W. Armstrong, J. W. Faust and W. A. Tiller, *J. Appl. Phys.*, 1960, **31**, 1954.
16 K. F. Hsu, S. Loo, F. Guo, W. Chen, J. S. Dyck, C. Uher, T. P. Hogan, E. K. Polychroniadis and M. G. Kanatzidis, *Science*, 2004, **303**, 818–821.
17 X. Z. Ke, C. F. Chen, J. H. Yang, L. J. Wu, J. Zhou, Q. Li, Y. M. Zhu and P. R. C. Kent, *Phys. Rev. Lett.*, 2009, **103**, 145502.
18 B. A. Cook, M. J. Kramer, J. L. Harringa, M. K. Han, D. Y. Chung and M. G. Kanatzidis, *Adv. Funct. Mater.*, 2009, **19**, 1254.
19 W. S. Liu, B. P. Zhang and T. Kita, *Appl. Phys. Lett.*, 2006, **88**, 092104.
20 B. A. Cook, M. J. Kramer, X. Wei, J. L. Harringa and E. M. Levin, *J. Appl. Phys.*, 2007, **101**, 053715.
21 J. R. Salvador, J. Yang, X. Shi, H. Wang and A. A. Wereszczak, *J. Solid State Chem.*, 2009, **182**, 2088–2095.
22 G. Kotuem, *Reflectance Spectroscopy*, Interscience, New York, 1969.
23 S. P. Tandon and J. P. Gupta, *Phys. Status Solidi*, 1970, **38**, 363.
24 M. K. Han, K. Hoang, H. Kong, R. Pcionek, C. Uher, K. M. Paraskevopoulos, S. D. Mahanti and M. G. Kanatzidis, *Chem. Mater.*, 2008, **20**, 3512.
25 K. Hoang, S. D. Mahanti, J. R. Salvador and M. G. Kanatzidis, *Phys. Rev. Lett.*, 2007, **99**, 156403.
26 S. Y. Wang, W. J. Xie, H. Li and X. F. Tang, *Intermetallics*, 2011, **19**, 1024.
27 J. P. Heremans, V. Jovovic, E. S. Toberer, A. Saramat, K. Kurosaki, A. Charoenphakdee, S. Yamanaka and G. J. Snyder, *Science*, 2008, **321**, 554.
28 D. G. Cahill, S. K. Watson and R. O. Pohl, *Phys. Rev. B: Condens. Matter Mater. Phys.*, 1992, **46**, 6131–6140.
29 J. Callayway and H. C. Von Baeyer, *Phys. Rev.*, 1960, **120**, 1149–1154.
30 P. G. Klemens, *Phys. Rev.*, 1960, **119**, 507–509.
31 B. Abeles, *Phys. Rev.*, 1963, **131**, 1906.
32 J. Yang, G. P. Meisner and L. D. Chen, *Appl. Phys. Lett.*, 2004, **85**, 1140.
33 H. J. Wu, S. W. Chen, T. Ikeda and G. J. Snyder, *Acta Mater.*, 2012, **60**, 6144–6151.
34 Y. Chen, M. D. Nielson, Y. B. Gao, T. J. Zhu, X. Zhao and J. P. Heremans, *Adv. Energy Mater.*, 2012, **2**, 58–62.